A STUDY OF THE AIR INLET EFFICIENCY OF A COMBAT AIRCRAFT CONCEPT WITH DORSAL INLET*

K. Widing
Senior Scientist
The Aeronautical Research Institute of Sweden (FFA)

Abstract

An experimental investigation has been carried out to increase the knowledge of the combined effects of the favourable wing flow and the disturbances from the forebody on the performance of a dorsal inlet concept at take off and landing conditions. Wind tunnel tests were performed with a 1:5 model in FFA's low speed wind tunnel. At the engine face station, both steady state and fluctuating pressure measurements were carried out to establish the inlet performance. A number of distortion indices for different engines have been calculated. Results are presented which indicate that both total pressure losses and distortion indices considered are relatively low and remain low up to moderate angles of attack and side-slip.

I. Introduction

For some years during the late 70's an extensive project work was carried out in Sweden, concerning a lightweight subsonic aircraft with combined attack and trainer capacity. This work covered a number of different configurations of which some to various degrees were unconventional, for example, characterized the position of the inlet on top of the fuselage. One of these co-called dorsal inlet configurations was studied at FFA and the object of this wind tunnel investigation was to find the inlet flow quality measured at a simulated engine face at take off and landing conditions.

Generally, the local flow angles at the inlet lips are dependent on the angle of attack, side-slip angle, flight speed and throttle position. The combined effect of these parameters often gives very high local flow angles at the inlet lips which could cause at least local separations. Still, the inlet system must provide air to the engine with low total pressure losses and a minimum of local disturbance at the engine face.

The basic idea is to reduce the effect of angle of attack by placing the inlet in the flow over the wing's upper surface where favourable effects could be expected, at least as long as the wing flow is not largely separated. On the other hand, the flow over the forebody, canopy, strakes, etc., is of course not at all independent of angle of attack (or side-slip) and the primary aim is, therefore, to increase the knowledge of the combined effects of the favourable wing flow and the disturbances from the forebody on the inlet performance.

During these project studies a number of suitable engines were of course considered. The question of inlet/engine compatibility arose at an early stage and therefore also the need for distortion indices. Unfortunately, no standard procedure is accepted by different engine manufacturers, which means that when several engines are of interest a large number of distortion indices have to be calculated.

To make a detailed inlet/engine compatibility analysis measurements are often needed with the engine face instrumented with a large number of high response pressure transducers. The purpose of this investigation has not been to generate instantaneous distortion indices. The simulated engine face of the scale 1:5 wind tunnel model shown in Figure 1 is instrumented to give ordinary steady distortion indices but also by use of three high response transducers to give some knowledge of the turbulence levels.

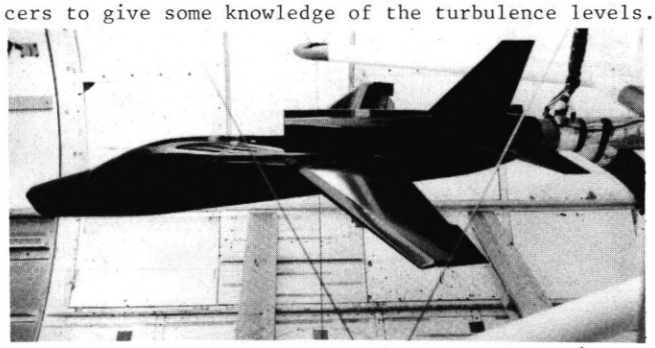

Figure 1. The 1:5 scale model installed in FFA's Low Speed Wind Tunnel.

* The investigation has been sponsored by the Swedish Defence Material Administration.

Design Features

Among the techniques for improving inlet flow condition the shielding either by wing, wing strakes or fuselage have been common and generally advantages have been found compared to an ordinary side-mounted inlet installation. One of the basic ideas is to find or create a flow field favourable for the inlet at high angles of attack and still keep the adverse effects of side-slip within tolerable limits.

A good example of this is the F-16 fighter design with its fuselage-shielded inlet. However, if the aircraft is to be operated from unprepared fields such a concept could be less good because of the risk of debris ingestion which probably should affect engine maintenance costs to an unacceptable level.

The present concept is characterized by the positioning of the inlet above the wing in the favourable flow over the wing's upper surface. Figure 2 illustrates the idea. A side-mounted inlet, dotted, is also indicated to show the large difference concerning the local flow angles at the lips of the inlets. The picture was taken at a preliminary flow test, model scale 1:25, in a smoke wind tunnel and at very low speed.

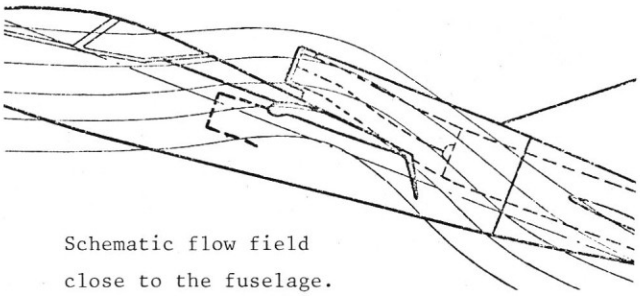

Schematic flow field close to the fuselage.

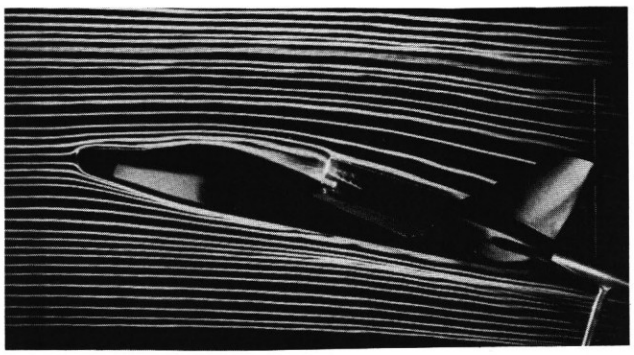

Figure 2. The favourable wing flow and a pretest in a smoke wind tunnel.

Other design features are summarized in Figure 3. The inlet is of ordinary pitot type positioned close to the wing's leading edge. The height of the canopy and the slope of the surface just ahead of the inlet is kept low to avoid too much overexpansion at high subsonic cruise Mach number. This area will then be supersonic and the intention is to minimize the risk for shock-induced boundary layer separation (Figure 3 a).

Two thin mini-strakes are included, (Figure 3 b), to prevent part of the fuselage side boundary layer reaching the area in front of the inlet. The vortices formed by the strakes removes this boundary layer flow. They are also intended to suck in some of the low energy air from the flow over the canopy and from the area at the top of the fuselage just in front of the inlet. The vortices pass outside the inlet and the geometry must be carefully chosen to prevent ingestion of a vortex into the inlet also at large angles of side-slip.

The underside of the forebody is a box-shaped section with relatively small radii at the corners (Figure 3 c). Compared to a round nose this lay-out gives a lower, more favourably located vortex pair. The vortices are also intended to give a considerable amount of downwash of boundary layer along the side of the fuselage.

To improve the inlet flow at large angles of side-slip a vertical wall located in the middle of the inlet is integrated in the duct design (Figure 3 d). The purpose is to facilitate the change of flow direction and to reduce the aerodynamic loading of the windward side of the inlet. This central wall is also intended somewhat to attenuate the unavoidable disturbances in the flow originating from the forebody.

From an aerodynamic point of view the central wall is probably unnecessarily long. The reason for the chosen length is to keep the possibility open for designing the wall of radar-absorbent material and as the duct often causes a large part of the radar cross-section area considerable reduction of this area may be achieved. It is also probable that the structural design of the duct could take advantage of this, giving weight reduction.

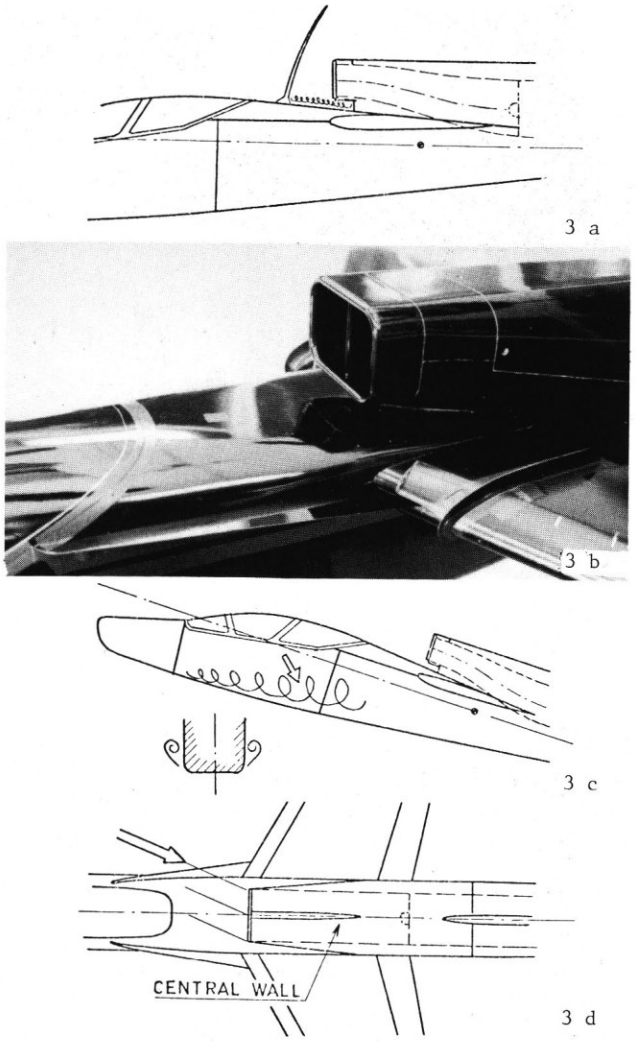

Figure 3. Some of the design features of the dorsal inlet concept.

As mentioned earlier the canopy's height must be kept low which affects the entire cockpit layout. It is, for instance, very important to try to avoid screening the pilot's visibility and a rather detailed study was made which prescribed a cockpit arrangement shown in Figure 4.

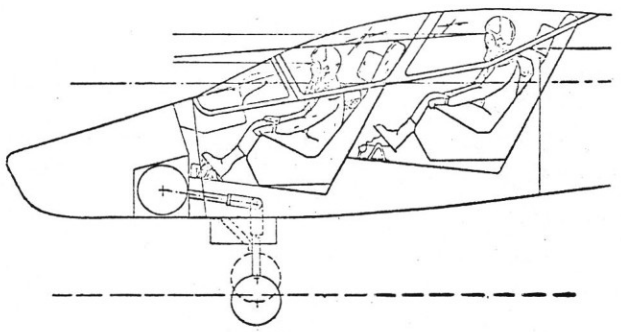

Figure 4. A possible cockpit arrangement.

Test Facility

The model was tested in the FFA's Low Speed Wind Tunnel. The wind tunnel is a continuous-operation closed-circuit wind tunnel with a 3.6 meter circular test section and a max. velocity of 95 m/sec. To generate the air flow through inlets the model is connected by a pipe-line to the large vacuum chamber system used for driving FFA's transsonic/supersonic wind tunnels. The capacity of the system is about 10 kg air per second permitting continuous test runs. As these tests include measurement of fluctuating total pressures the turbulence level at the test section expressed as $\Delta_{p_{RMS}}/p_{o_\infty}$ was determined. At a velocity of 70 m/sec. an average value of 0.03% was found, which is more than adequate for these tests.

Model Description

The model is shown in Figure 1. The scale of the model is 1:5 of a 9 meter span aircraft. The forebody with its flat FLIR nose and with the two-seat tandem cockpit is a possible aircraft geometry but most of the aft part of the model is to some extent schematic. The 25^0 swept wing is equipped with movable leading and trailing edge flaps and a small strake is placed in front of the wing. The wing has a symmetric profile with a thickness of 10%. The external contours of the model are shown in Figure 5.

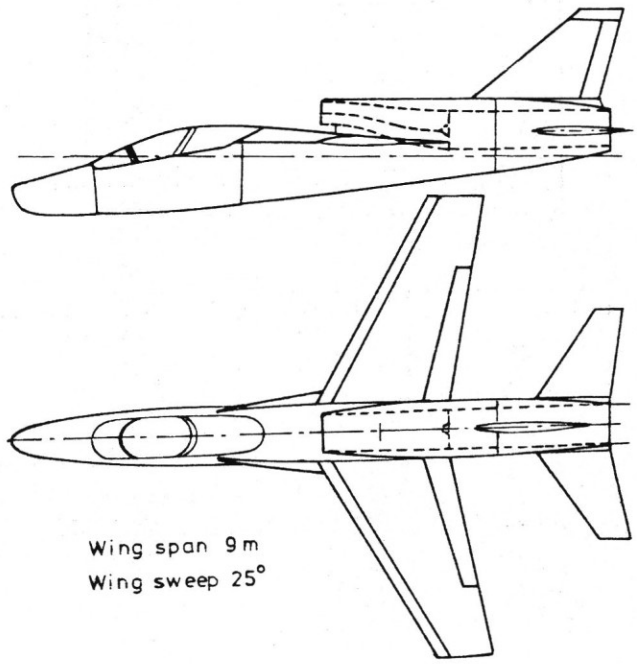

Figure 5. The aircraft layout.

The inlet/duct arrangement is shown in Figure 6, where also the size and position of the central wall is shown.

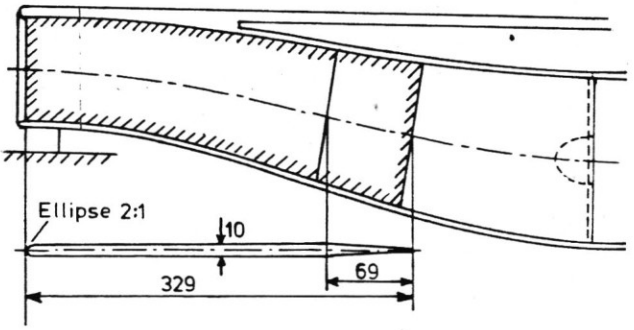

Figure 6. Inlet/duct arrangement.

Two of the three inlets tested, Figures 7 and 8, have basically the same shape. The difference is the lip section where inlet 3 has a symmetrical elliptic section, while inlet 4 is non-symmetric to give a larger inner radius. Characteristic for inlet 5 is its considerably sharper and extended upper lip giving a 20^0 inclined inlet opening. The lower lip section is the same as inlet 4 and the radius along the side wall of the inlet decreases continuously upwards.

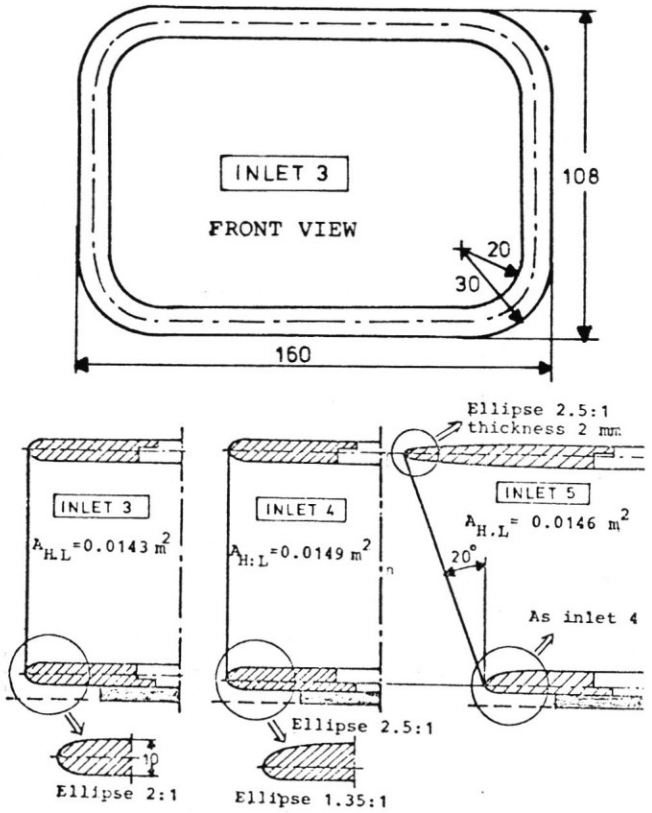

Figure 7. The geometry of inlet 3, 4 and 5.

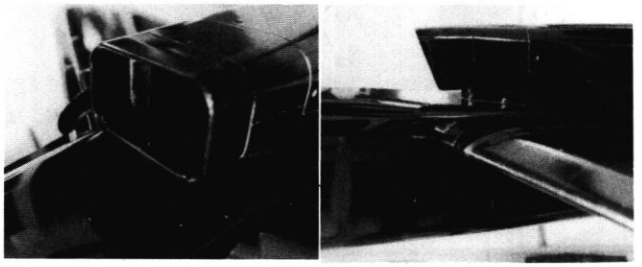

Figure 8. The shape of inlets 3 and 5.

The duct is S shaped, has constant width and sections built up of straight lines and rounded corners. The corner radius is continuously increasing towards the simulated engine face. The entire available length has been used to form an S shape with as little curvature as possible. Figure 9 shows the general arrangement and the area distribution.

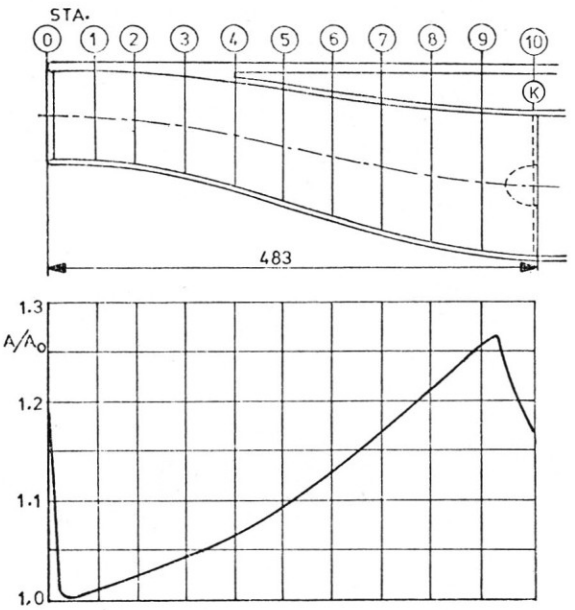

Figure 9. The area distribution of the duct. (Without the effect of the central wall).

Model Instrumentation

The model was instrumented to obtain both steady state and high-response pressures at the simulated engine face station. The six-arm rake shown in Figure 10 was rotatable and remotely controlled. Five of the six arms were equipped with six ordinary total pressure probes each. High-response data giving the turbulence levels in the flow were obtained from three transducers (Kulite XCQL-20-093-25) located at the sixth arm. Each probe was positioned in the centre of equal, annular, areas.

During a test run the rotatable rake was stepped giving steady-state data at increments of 15^0 and turbulence data at increments of 30^0. Also four static pressure taps were located at this station used for calculating average dynamic pressure and rate of air flow through the inlet.

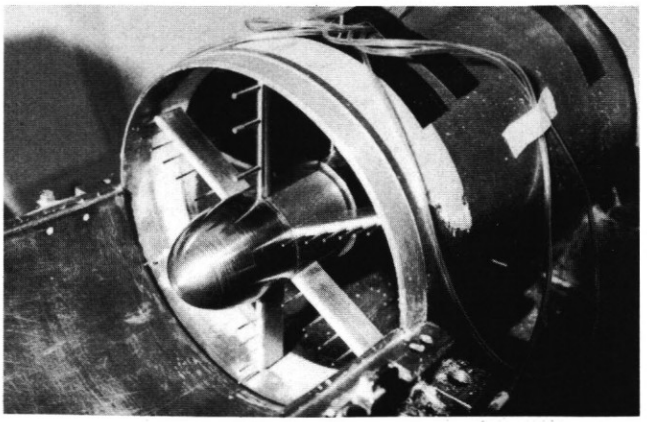

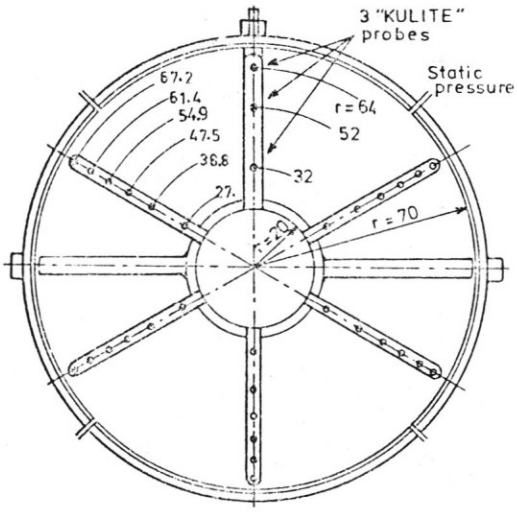

Figure 10. The rotatable and remotely-controlled rake system.

Data Acquisition

A block diagram of the data acquisition system is shown in Figure 11. The system used to evaluate inlet performance consists of two parts; a low response recording system and a high response recording system.

The steady state data were recorded with an ordinary computer-controlled scanivalve system. The signals were filtered through a 18 dB/octave LP filter with an upper cut off frequency of 7 Hz prior to sampling.

The unsteady pressure signals from the Kulite transducers are amplified and divided into two branches of which one stores the signals on analog tape for later analysis and the other carries the signals through preselected filters to the on-line RMS meters. It was assumed that the engine reacts to fluctuations lasting longer than the time required for one engine rotor revolution. The upper cut off frequency of the 24 dB/octave filters were after linear scaling (5:1) set to 1000 Hz corresponding to approx. max. engine r.p.m. The signals were also examined by a power spectral density (PSD) analyzer so that for instance root mean square values from the RMS meters could be compared. Final results were obtained from the FFA central computer.

Results and Discussion

An investigation concerning a number of configurations, various angles of attack, angles of sideslip and inlet mass flows gives a very large amount

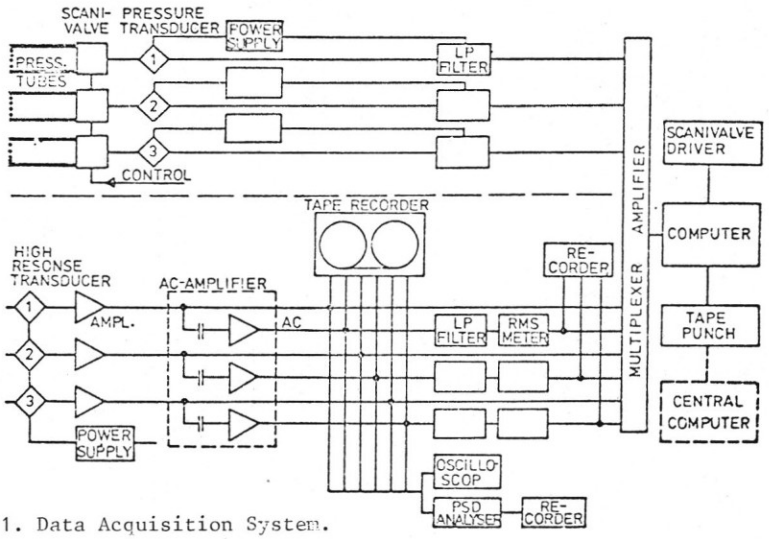

Figure 11. Data Acquisition System.

of data and only the main results are presented here. The conditions at the simulated engine face are in general described by total pressure losses (f), steady state distortion indices (DC_{60}) and turbulence levels ($TU_{C_{60}}$) .

The tests were carried out at a free stream Mach number of 0.18 and all the results apply to a take off/landing configuration with leading edge flaps at 20^0 and the double slotted trailing edge flaps at 50^0. The discussion is divided into 2 parts:

1. Effects of various configuration changes.
2. A more detailed presentation of the results from a selected configuration (Conf. 20, inlet 4).

Figure 12 shows the effects of the different shapes of inlets 3, 4 and 5 on total pressure losses and distortion. Inlet 4 is obviously in all respects the best one. To examine the flow over the inlet lips in detail, oil flow tests were carried out. These tests showed that the windward lower corner became critical when increasing angle of side-slip. Comparing the geometry of inlets 3 and 4 (Figure 7) the larger inner profile radius of inlet 4 causes less lip separation, explaining the better results. Comparing inlets 4 and 5, both having the same geometry at the lower corners, oil flow test showed that the sharper side wall of inlet 5 was responsible for the higher losses and distortions at high side-slip angles. It should be observed that the mass flow ratio is at its maximum value (MFR = 2.2) so that the inlet lips even at $\alpha/\beta = 0$ are heavily loaded aerodynamically.

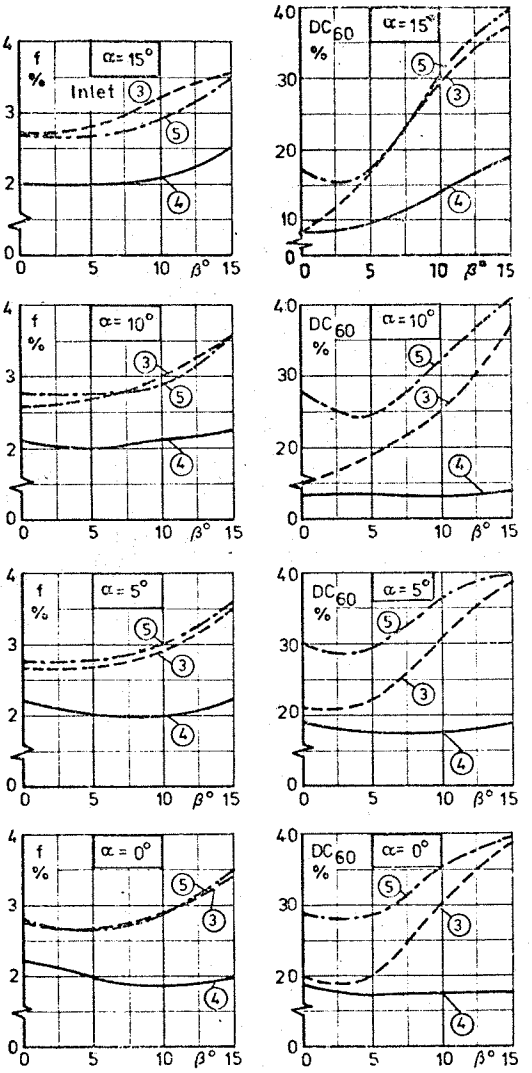

Figure 12. Steady state data for inlets 3, 4 and 5 MFR = 1.0 .

In Figure 13 the turbulence levels for inlets 4 and 5 are shown. (Turbulence results from inlet 3 are not available). Often high DC_{60} values correspond to high $TU_{C_{60}}$ values, but that this is not always true is obvious when comparing the results at 15^0 angle of attack.

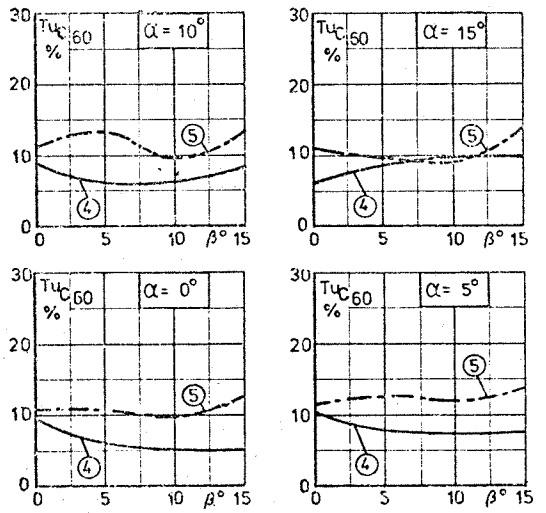

Figure 13. Turbulence levels for inlets 4 and 5 MFR = 2.2 .

Figures 14 and 15 show the effect of the mini-strakes. At high mass flow ratios and at 15^0 angle of side-slip its main effect is in reducing the total pressure losses. At low mass flow ratios (MFR=1) the strakes reduce the distortion significantly both at high angles of attack and side-slip. This indicates that in manoeuvers at higher speeds the strakes will have a favourable effect on inlet distortion.

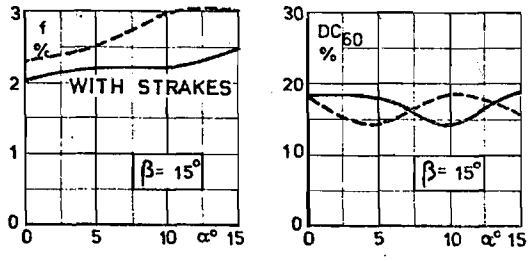

Figure 14. Effects of the strakes at MFR = 2.2 .

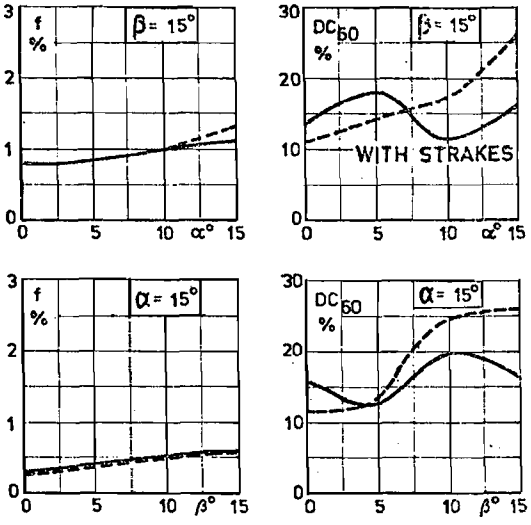

Figure 15. Effects of the strakes at MFR = 1.0 .

Figures 16 and 17 show the effect of the central wall at 0^0 and 10^0 angle of attack and at various side-slip angles. The wall is relatively large (geometry Figure 6) and it evidently increases the total pressure losses due to skin friction and probably also by corner interaction effects with the duct walls. However, the intended purpose to reduce the effect of the angle of side-slip is clearly shown both at high and low mass flow ratios.

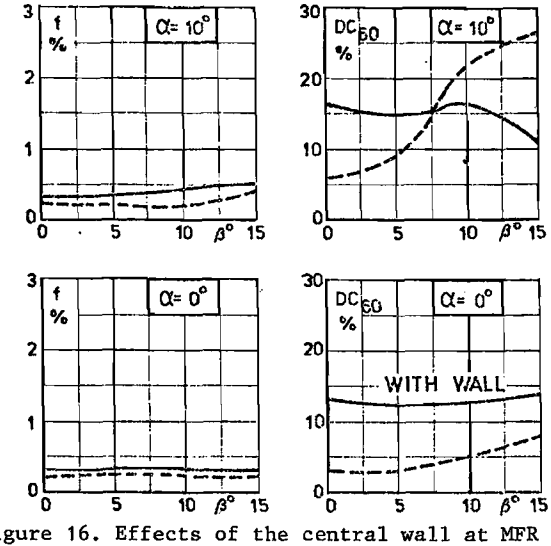

Figure 16. Effects of the central wall at MFR = 1.0

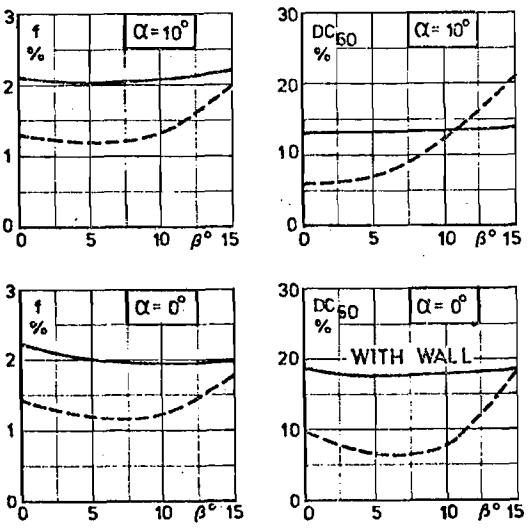

Figure 17. Effects of the central wall at MFR = 2.2 .

Configuration 20

This configuration is made up of inlet 4, strakes and central wall and has been more carefully examined and also the α and β ranges have been extended to 20^0. The wing is completely stalled at about 17^0 angle of attack when fitted with stall fences (otherwise the wing stalls at about 12^0), which means that results presented at 20^0 angle of attack at various side-slip angles are with the aircraft in a post-stalled condition. Some of the results are summarized in Figure 18. Concerning the total pressure losses (f) the figure shows that they are generally at a low level and only slightly increase with angle of attack and side-slip. It is well-known that combining steady state with turbulence data (RMS values) could be very hazardous and that the results obtained depend on the procedure used. Despite that a combined index is formed here, called $DC60_{PEAK}$, by simply adding steady state and turbulence data at the worst 60^0 sector of the engine face. Both this peak index and the steady state DC_{60} index are shown in the figure. The $DC_{60\ PEAK}$ index ought to give some information of the order of magnitude of the turbulence effects on the distortion.

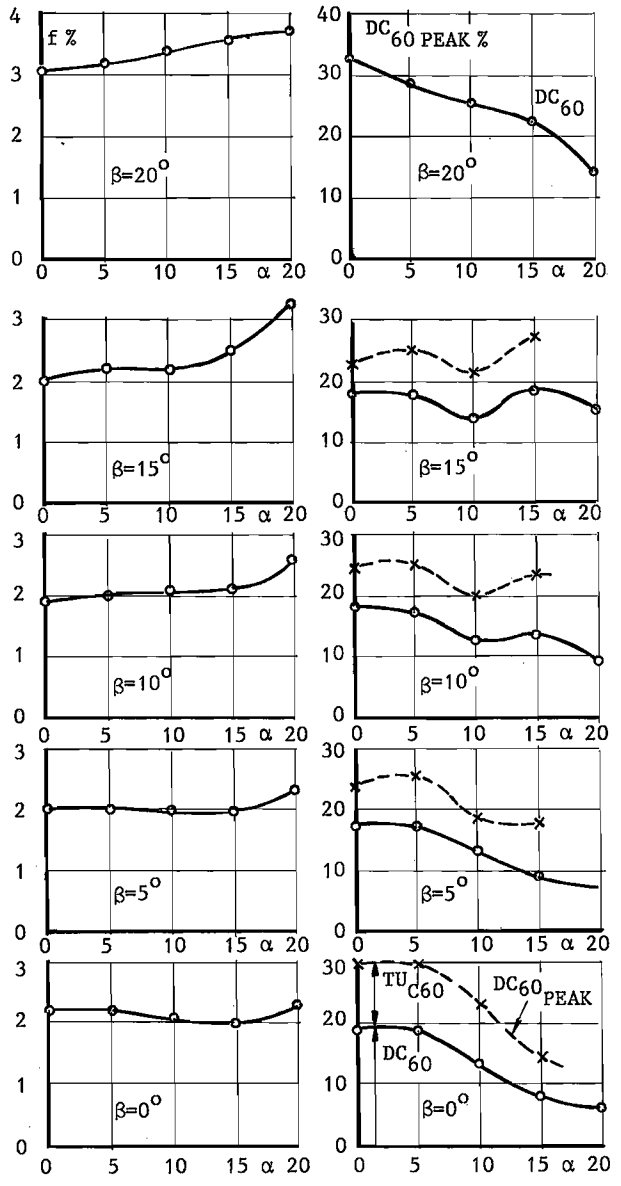

Figure 18. Results obtained with Configuration 20 at MFR = 2.2 .

Figure 19 shows, as an example, correlations between steady state and turbulence measurements. Large RMS values are found near low total pressure areas but a closer examination shows that maximum RMS values often occur where the pressure gradient is largest.

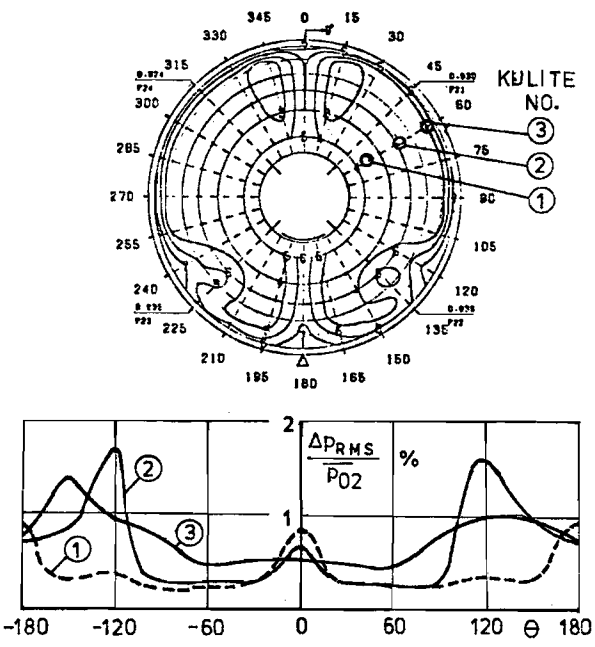

Figure 19. An example of correlations between steady state and turbulence measurements.

Earlier presented basic performance expressed as total pressure losses and distortion indices showed that this configuration is not very sensitive to changes in either angle of attack or side-slip. However, that this is not the case is obvious when studying the distortion patterns at the engine face shown in Figure 20. The isobars in this figure show constant local total pressure in relation to mean pressure and the step between two lines is 0.025 . These patterns, including the worst combinations of α and β of the test program show large differences in flow conditions.

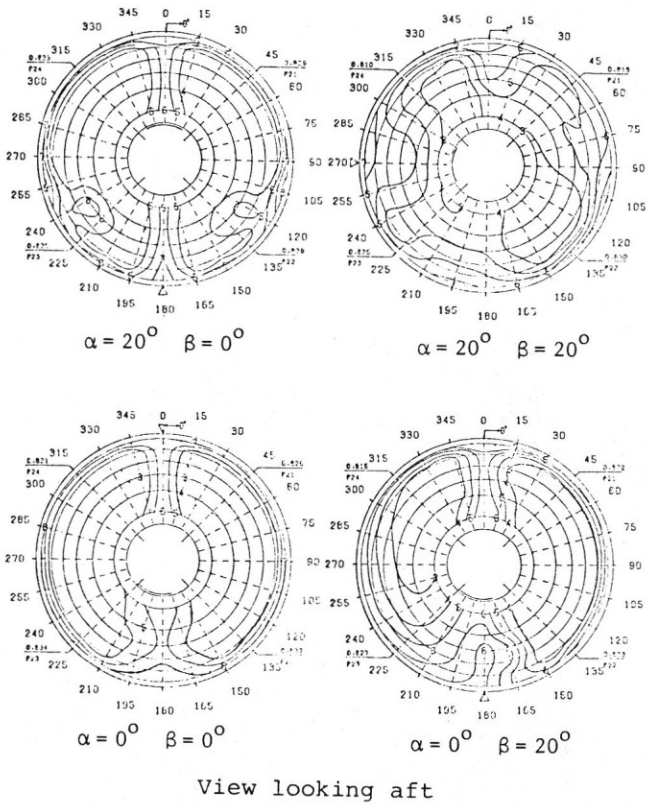

Figure 20. Example of distortion patterna obtained with configuration 20 at MFR = 2.2 .

Flow studies using tufts were also made and Figure 21 shows an example at 20^0 angle of attack and zero side-slip. In front of the inlet the flow is attached and also visible are traces from the vortices generated by the strakes.

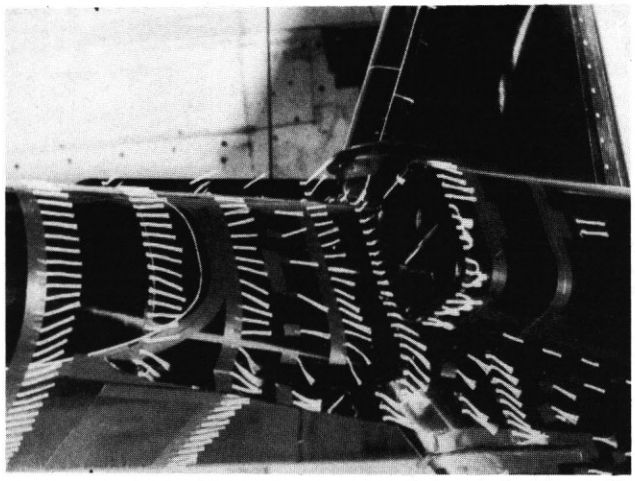

Figure 21. Flow visualization at 20^0 angle of attack and at maximum mass flow ratio.

Distortion Index Discussion

As mentioned earlier different engine manufacturers use their own set of distortion indices. The DC_{60} index so far presented is commonly used in connection with Rolls Royce engine performance data. Pratt & Whitney Aircraft often uses relatively complex indices combining circumferential and radial distortions defined for example for the fan as

$$K_{A2} = K_{\theta} + bK_{RA2}$$

K_{A2} and K_{RA2} have been calculated separately and the results are shown in Figure 22. Also General Electric uses a combined index and defined this as

$$ID = b \times K_c \times IDC + K_R \times IDR$$

Here the IDC and IDR values have been calculated and are shown in Figure 23.

All the distortion indices presented are considered low. This expression gets its full meaning first when complete and combined indices can be obtained and be related to the limits and especially to the stall margin of the engines considered. This is tru especially when studying more unconventional aircraft concepts where the inlet/engine compatibility could be of critical importance for the entire project.

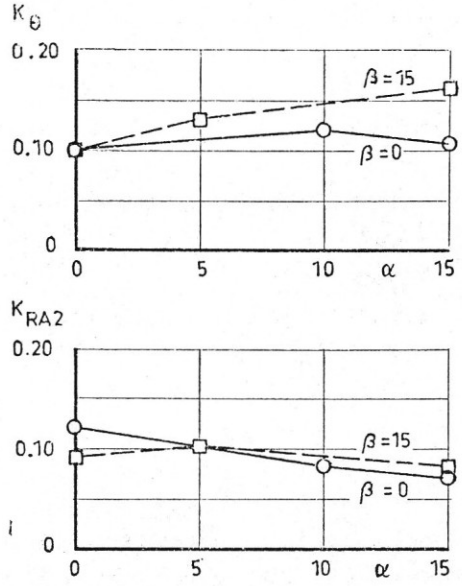

Figure 22. Steady state distortion indices (PWA).

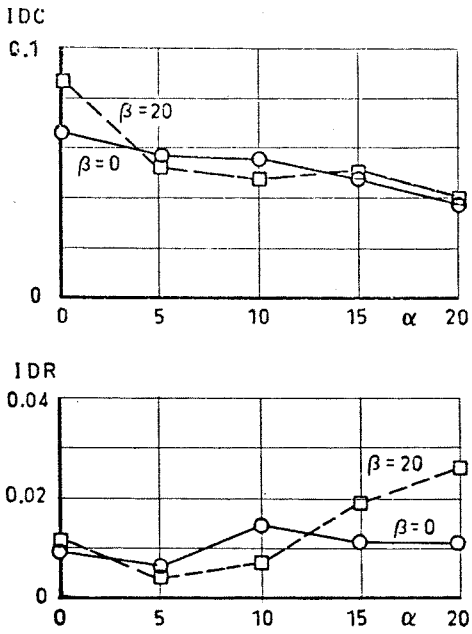

Figure 23. Steady state distortion indices (GE).

Conclusions

This wind tunnel investigation has shown that an aircraft concept characterized by the inlet mounted on top of the fuselage can be designed to give good inlet performance at low speed under take off and landing conditions. Both total pressure losses and distortions have shown to be rather unaffected by angle of attack and side-slip up to at least 20^0. It has also been shown, especially by flow studies that the design of the forebody is very important and must be made with great care to match the chosen inlet position. Furthermore, despite the fact that the simulated engine face has not been fully instrumented with high response transducers the information from the turbulence measurements has been very useful when considering the complex flow at the engine face.

The investigation will be continued at high subsonic speeds.

Acknowledgements

The author gratefully acknowledges the support from Bo Bengtsson, Lars-Inge Nilsson and Sören Stridsberg in performing the extensive wind tunnel testing.

Some definitions

TOTAL PRESSURE LOSSES:

$$f = \frac{p_{o_\infty} - \overline{p_{o_K}}}{\overline{p_{o_K}}}$$

DISTORTION INDEX:

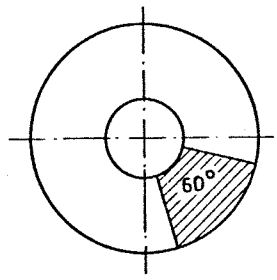

$$DC_{60} = \frac{\overline{p_{o_K}} - (\overline{p_{o_{60}}})_{MIN}}{\overline{q}_K}$$

$$TU_{C_{60}} = \left[\frac{\Delta p_{RMS60}}{\overline{q}_K}\right],$$

$$DC_{60_{PEAK}} = DC_{60} + TU_{C_{60}}$$

$\overline{p}_{o_K}$ = Average engine face total pressure

$\overline{q}_K$ = Average engine face dynamic pressure

MASS FLOW RATIO:

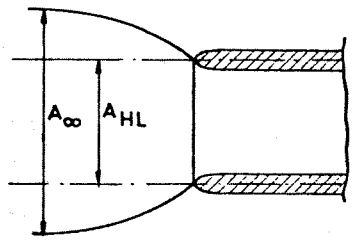

$$MFR = \frac{MASSFLOW}{\rho_\infty U_\infty A_{HL}} = \frac{A_\infty}{A_{HL}}$$